

Contents lists available at ScienceDirect

Insect Biochemistry and Molecular Biology

journal homepage: www.elsevier.com/locate/ibmb



Efficient entry of budded virions of Autographa californica multiple nucleopolyhedrovirus into *Spodoptera frugiperda* cells is dependent on dynamin, Rab5, and Rab11



Qi Yue^a, Jingfeng Li^a, Ya Guo^{a,1}, Fanye Yan^a, Ximeng Liu^a, Gary W. Blissard^b, Zhaofei Li^{a,*}

^a State Key Laboratory of Crop Stress Biology for Arid Areas, Key Laboratory of Integrated Pest Management on Crops in Northwestern Loess Plateau, Ministry of Agriculture, College of Plant Protection, Northwest A&F University, Yangling, Shaanxi, 712100, China

ARTICLE INFO

Keywords: AcMNPV Baculovirus Dynamin Rab5 Rab11

ABSTRACT

Autographa californica multiple nucleopolyhedrovirus (AcMNPV), a member of the *Alphabaculovirus* genus of the family *Baculoviridae*, is an enveloped double-stranded DNA virus. Budded virions (BVs) of AcMNPV enter host cells via clathrin-mediated endocytosis. However, the route of functional intracellular trafficking of AcMNPV BVs during entry is not well established. In the current study, we found that entering BVs were colocalized mainly with cellular Rab5 and Rab11. Expression of dominant-negative (DN) Rab5 and Rab11 or RNAimediated down regulation of these two cellular transcripts significantly reduced BVs entry into but not egress from *Spodoptera frugiperda* cells (Sf9), whereas similar treatments for Rab4 and Rab7 had no apparent effect on virus infection. Combined with data from RNAi knockdowns of dynamin, and dynasore inhibition assays, our results support a model in which AcMNPV BVs enter permissive host cells by clathrin-mediated endocytosis, followed by de-envelopment of BVs predominantly within early and maturing endosomes rather than within late endosomes. Additionally, Rab11 suppression studies suggest the Rab11-dependent recycling endosomal pathway is involved in virion entry.

1. Introduction

Autographa californica multiple nucleopolyhedrovirus (AcMNPV) is a member of the Alphabaculovirus genus of the family Baculoviridae. Baculoviruses comprise a large group of enveloped and double-stranded DNA viruses that infect insects in the orders Lepidoptera, Diptera, and Hymenoptera (Harrison et al., 2018). They are used as biological insecticides and as important vectors for expressing proteins or transducing mammalian cells (Chambers et al., 2018; Rohrmann, 2019). In an infection cycle, baculoviruses such as AcMNPV produce two distinct virion phenotypes: occlusion-derived virions (ODVs) and budded virions (BVs). ODVs and BVs differ in that their envelopes are derived from plasma membrane (BVs) or intranuclear microvesicles (ODVs). In insects, ODVs target the midgut epithelial cells and initiate infection there. Then, newly generated BVs bud from the basolateral plasma membrane of the midgut cells into the hemocoel and spread the infection within the majority of tissues. In permissive cell culture systems, BVs (but not ODVs) can efficiently initiate and spread the virus infection, even though both of types of virions are assembled and produced in cultured cells (Blissard and Theilmann, 2018; Rohrmann, 2019)

BVs of AcMNPV enter permissive host cells via clathrin-mediated endocytosis (Long et al., 2006; Volkman and Goldsmith, 1985). Prior studies demonstrated that the entry of BVs is dependent on the acidic pH within endosomes (Hefferon et al., 1999), which triggers a conformational change of the viral protein GP64. GP64 then mediates the fusion of the viral envelope and endosome membranes to release the nucleocapsid into the cytosol (Blissard and Wenz, 1992; Hefferon et al., 1999; Kadlec et al., 2008). In the cytosol, the nucleocapsids are delivered to, and enter the nucleus by a propulsion system that involves virus-induced actin polymerization (Goley et al., 2006; Mueller et al., 2014; Ohkawa et al., 2010). Following the assembly of new viral capsids in the nucleus, one subset of nucleocapsids egress across the nuclear membrane into the cytosol, and then are transported to and bud at the plasma membrane to form BVs. Another subset of nucleocapsids is retained within the nucleus where they are enveloped to form ODVs

^b Boyce Thompson Institute, Cornell University, Ithaca, 14853, New York, USA

^{*} Corresponding author. College of Plant Protection, Northwest A&F University, Taicheng Road, Yangling, Shaanxi, 712100, China. E-mail address: zhaofeili@nwsuaf.edu.cn (Z. Li).

¹ Department of Entomology and Nematology, University of Florida, Gainesville, Florida, 32,611.

Table 1 PCR primers.

Primer name	Sequence (5' to 3')	Description
Rab4BF	aatggatccatgtctgaatcctacgaatact	Amplification of the ORF of rab4, rab5, rab7, and rab11 and their site-mutation constructs
Rab4ER	aatgaattctcatacatggcaggcacaatcaga	
Rab5BF	aatgaattcatggcgaccaacaggagcggtgc	
Rab5ER	aatgaattctcacttgcagcaggaggaggagg	
Rab7BF	aatggatccatgtcgtcgagaaagaaggca	
Rab7ER	aatgaattcctagcaagcacagttgtcaccatc	
Rab11BF	tatggatccatgggcacaagaggaggacgaatac	
Rab11ER	atagaattcctactggcagcactgcttgcgcac	
Rab4 ^{N121I} F	attaagaaggatatggaagaatcaagagaagtcaca	
Rab4 ^{N121I} R	tgattcttccatatccttcttaatccccacaagtaaa	
Rab5 ^{S36N} F	aattegetggtgetgegettegtgaa	
Rab5 ^{S36N} R	aagcgcagcaccagcgaattcttgccca	
Rab7 ^{T22N} F	aactcgcttatgaatcagtttgtcaacaagaa	
Rab7 ^{T22N} R	gacaaactgattcataagcgagtttttgcctacaccgct	
Rab11 ^{S25N} F	aatagtctcctatcacgtttcactcgaaatga	
Rab11 ^{S25N} R	agtgaaacgtgataggagactatttttaccgactccaga	
DynF	tgccttggtgtctggtctcttga	Amplification of a small fragment of dynamin, rab4, rab5, rab7, and rab11 for quantitative real-time PCR
DynR	ggtgccgttcatctgtggagttg	implication of a small regiment of alymphotology, and it would be quantitative real time to the
Rab4QF	aatcgtgaacataggcggcaagtc	
Rab4QR	gttctagcgtctcggagccaattc	
Rab5QF	gagtcagcagtgggcaagtcttc	
Rab5QR	cagtggtgtcatcgaggcatacg	
Rab7QF	tcatccttggcgatagcggtgta	
Rab7QI Rab7QR	gcctattgttgccttgtactggttg	
Rab11QF	gccaagcatctgtcctacgagaac	
Rab11QF Rab11QR	aggtgcctaagatcgctcttgttac	
Dyn1dsF	ggatcctaatacgactcactatagggaggtgccaattggagatcag	Amplification of the dsDNA of gfp, dynamin, rab4, rab5, rab7, and rab11. The T7 promoter sequence is
Dyn1dsR Dyn1dsR	ggatcc <u>taatacgactcactataggg</u> aggigccaatiggagatcag ggatcc <u>taatacgactcactataggg</u> ttgcttcgtctttgagagca	underlined.
Dyn1dsK Dyn2dsF		undermed.
•	ggatcc <u>taatacgactcactatagggg</u> ccgcaccttagattccata	
Dyn2dsR	ggatcc <u>taatacgactcactataggg</u> ccaaattttccaccatagcg	
GFPdsF	ggatcctaatacgactcactatagggacgtaaacggccacaagttc	
GFPdsR	ggatcctaatacgactcactatagggtgttctgctggtagtggtcg	
Rab4dsF	ggatcctaatacgactcactatagggaaaatcgtgaacataggcgg	
Rab4dsR	ggatcc <u>taatacgactcactataggg</u> ctaagcctctttgacgtgcc	
Rab5dsF	ggatcc <u>taatacgactcactataggg</u> gccacagacgaaagtatgcc	
Rab5dsR	ggatcc <u>taatacgactcactataggg</u> ccttcacccagttcttggc	
Rab7dsF	ggatcc <u>taatacgactcactataggg</u> tccaatctttaggagtggcg	
Rab7dsR	ggatcc <u>taatacgactcactataggg</u> cacagttgtcaccatccctg	
Rab11dsF	ggatcctaatacgactcactataggggatcacgtcggcgtactacc	
Rab11dsR	ggatcctaatacgactcactataggggcgcatctgcttctgagatac	
ODV-e56F	gatcttcctgcgggccaaacact	Amplification of a 183 bp fragment of AcMNPV ODV-e56
ODV-e56R	aacaagaccgcgcctatcaacaaa	

(Blissard and Theilmann, 2018). Several studies found that cellular components of the endosomal sorting complex required for transport (ESCRT) and the soluble *N*-ethylmaleimide-sensitive factor (NSF) attachment protein receptor (SNARE) system are necessary for efficient entry and egress of BVs (Guo et al., 2017; Li and Blissard, 2012; Yue et al., 2018). However, the precise mechanism of endosomal trafficking of BVs that occurs following internalization from the cell surface remains unclear.

While some enveloped viruses enter cells by fusing directly with the plasma membrane, most exploit cellular endocytosis to deliver their genetic contents into the cell. The most common route of enveloped virus internalization is clathrin-mediated endocytosis (CME) (Mercer et al., 2010). A typical CME pathway consists of a few sequential but partially overlapping steps, including cargo recruitment, vesicle scission, trafficking, vesicle fusion with the early endosome (EE) (Kaksonen and Roux, 2018). At the plasma membrane, endocytic vesicles are constricted and scission is catalyzed by a GTPase, dynamin (Antonny et al., 2016). Vesicle trafficking, fusion with EE, and endosomal trafficking are tightly regulated by a group of small Rab (Ras-related protein in brain) GTPases (Goody et al., 2017; Huotari and Helenius, 2011). Of these, Rab4, Rab5, Rab7, and Rab11 function as major molecular switches to control endocytic vesicle trafficking. Rab5 is localized primarily on EE and regulates endocytic vesicle formation and trafficking from the plasma membrane to EE and homotypic fusion of EE. Rab4 and Rab11 are both involved in regulating of endocytic cargos recycling from EE back to the plasma membrane. Rab4 is mainly present on EE and controls fast recycling of cargos back to the cell surface, whereas Rab11 is localized on recycling endosomes (RE) and regulates a slow recycling pathway to deliver the cargos to the plasma membrane (Goody et al., 2017; Huotari and Helenius, 2011). Rab7 is mainly localized to late endosomes (LE) and controls the transition of EE to LE and regulates the trafficking within LE and to lysosomes (Goody et al., 2017; Huotari and Helenius, 2011). Prior studies reveal that the entry of many DNA and RNA viruses requires Rab5, Rab7 and/or Rab11 (Mercer et al., 2010). Also, Rab11 is necessary for assembly or release of some DNA and RNA viruses (Bruce et al., 2012; Vale-Costa and Amorim, 2016).

To investigate internalization and endosomal trafficking of BVs of AcMNPV in *Spodoptera frugiperda* Sf9 cells, we used a variety of approaches including: a chemical inhibitor of dynamin; RNAi of *dynamin* and *rab* genes *rab4*, *rab5*, *rab7*, and *rab11*; and DN constructs of Rab4, Rab5, Rab7, and Rab11. Our results indicate that efficient entry of BVs into Sf9 cells is dependent on dynamin, Rab5, and Rab11. We propose that membrane fusion and nucleocapsid release into the cytosol may occur predominantly within EE and maturing endosomes, prior to the Rab7-associated late endosomal compartment. Additionally, our results suggest that the Rab11-dependent recycling endosomal pathway is involved in virion entry.

2. Materials and methods

2.1. Cells, viruses, and reagents

Sf9 cells were maintained at 27 °C in TNMFH medium (Sigma-Aldrich) supplemented with 10% fetal bovine serum (Gibco). Two recombinant AcMNPV viruses that contained a) two reporter genes: LacZ and GUS (AcMNPV-LacZGUS) (Yue et al., 2018), or b) mCherry-labeled major capsid protein VP39 (AcMNPV-3mC) (Ohkawa et al., 2010), were propagated and titered in Sf9 cells. Cells in 12-well plates (2 \times 10 5 cells per well) or 6-well plates (1 \times 10 6 cells per well) were transfected with a CaPO $_4$ precipitation method. For virus infection, after a 1 h incubation of cells with the virus, the inoculum was removed and the cells were washed once with TNMFH medium. The dynamin inhibitor, dynasore, was dissolved in dimethyl sulfoxide (DMSO) (Sigma Aldrich).

2.2. BVs purification

BVs were purified as described previously (Guo et al., 2017). Sf9 cells in T75 flasks were infected with AcMNPV-3mC or AcMNPV-LacZGUS (MOI = 5). At 96 h post-infection (p.i.), the cell culture supernatants were harvested and BVs were collected through a 25% (wt/vol) sucrose cushion by centrifugation at 4 °C, 28,000 rpm for 90 min (Himac CP100WX, HITACHI). Virus pellets were resuspended in TNMFH medium and isolated with a 30–55% (wt/vol) continuous sucrose gradient under the same centrifugation condition. The virus fraction was collected, diluted with TNMFH medium, and centrifuged as above. BVs pellets were resuspended in TNMFH medium and then sterilized with a syringe filter ($\Phi = 0.45~\mu m$, PALL Life Sciences), the virus titer was determined by 50% tissue culture infection dose (TCID₅₀) assays.

2.3. cDNA cloning

Total RNA was isolated from Sf9 cells using an RNAiso plus kit (TaKaRa), and then reverse-transcribed into cDNA with an RNA LA PCR kit (TaKaRa). Gene-specific primers (Table 1) targeted to the open reading frame (ORF) of *rab* genes and the partial fragments (*dynamin*: 90 bp; *rab4*: 180 bp; *rab5*: 124 bp; *rab7*: 92 bp; *rab11*: 113 bp) within ORF of *dynamin* and *rab* genes were designed based on the transcriptome shortgun assembly (TSA) database of *Spodoptera frugiperda* (https://www.ncbi.nlm.nih.gov/bioproject/PRJNA318819). PCR-amplified fragments were separately inserted into pMD18-T vector (TaKaRa) and confirmed by sequencing.

2.4. Analysis of the transcription of dynamin and rab genes

Sf9 cells in 6-well plates were infected with AcMNPV-LacZGUS (MOI = 5). At different times (1–48 h) p.i., total RNA was isolated from the infected and uninfected control cells by using an RNeasy Mini Kit (QIAGEN). After eliminating the genomic DNA with gDNA eraser in PrimeScript™ RT reagent kit (TaKaRa), the cDNA was reverse-transcribed with an oligo-dT primer (TaKaRa). The transcript of *dynamin* and *rab* genes was measured by quantitative real-time PCR (qPCR) (CFX96 Touch™ real-time PCR system, Bio-Rad). Each PCR mixture contained 10 µl SYBR® Premix ExTaq II (TaKaRa), 2.5 µM each primer (Table 1), and 800 ng of the cDNA template. Thermal cycling conditions were one cycle of 95 °C for 3 min, followed by 40 cycles of 95 °C for 10s, and 60 °C for 30s. A standard curve for each gene was generated by a serial dilution of pMD18-T vector containing a small fragment of *dynamin* or *rab* genes. The transcript levels of each gene were expressed as numbers of transcript copies per cell.

2.5. Mutagenesis and construction of plasmids and bacmids

Site-directed mutagenesis was performed with overlap PCR (Primers

see Table 1) using a pMD18-T vector that contained each *rab* gene, to separately introduce single amino acid mutation N121I, S36N, T22N, or S25N into Rab4, Rab5, Rab7, or Rab11, respectively. PCR products were digested with BamHI and EcoRI and inserted into the plasmid pIEnGFP (Yue et al., 2018) to produce the target genes fused with GFP at the N-terminus and generate the transient expression plasmid GFP-Rab4^{N121I}pBlue, GFP-Rab5^{S36N}pBlue, GFP-Rab7^{T22N}pBlue, and GFP-Rab11^{S25N}pBlue. The ORFs of wild-type (WT) Rab4, Rab5, Rab7, and Rab11 were isolated from a pMD18-T plasmid that contains each *rab* gene by digestion with BamHI and EcoRI, and then inserted into pIEnGFP to generate GFP-Rab4pBlue, GFP-Rab5pBlue, GFP-Rab7pBlue, and GFP-Rab11pBlue. The GFP expression plasmid GFPpBlue (Li and Blissard, 2012) was used as a control.

To generate recombinant AcMNPV bacmids that expressed GFP and GFP-tagged Rab5 and Rab11 (WT or with mutations), a fragment containing the AcMNPV *ie1* promoter and GFP or GFP-fused WT or mutated *rab5* and *rab11* was isolated from the above transient expression plasmids and inserted into a pFastbac plasmid GUSpFB (Yue et al., 2018), which contained a reporter gene GUS under the AcMNPV *p6.9* promoter. The resulting pFastbac constructs were each inserted into an AcMNPV bacmid (bMON14272) as described previously (Luckow et al., 1993). Recombinant bacmids were separately named GFP-Bac, GFP-Rab5-Bac, GFP-Rab11-Bac, and GFP-Rab111-Bac, and GFP-Rab111-Bac. The transient expression plasmids and bacmids were extracted by using a Midiprep kit (Invitrogen).

2.6. Cell viability assay

Cell viability, upon treatment with the dynamin inhibitor dynasore, or expression of WT or mutated Rab proteins, was assessed using the CellTiter96 AQueous One Solution Cell Proliferation Assay kit (Promega). Briefly, Sf9 cells in 12-well plates were cultured in TNMFH medium containing varying concentrations of dynasore (5–50 μ M) for 3 h or transfected with 2 μ g of the plasmid expressing GFP or GFP-tagged Rab proteins. At 3 h post-treatment with the drugs or at 16 h post-transfection (p.t.), the cells were incubated with CellTiter 96 AQueous One Solution reagent for 2 h at 27 °C and absorbance at 490 nm was monitored using a 96-well plate reader (Tecan iControl Reader, Mannedorf).

2.7. Dynamin inhibition assay

The dynamin inhibition assay was performed as described previously with modifications (Lee et al., 2013). Sf9 cells in 12-well plates were pre-treated with dynasore (5–20 μ M) for 3 h. After removing the drugs, the cells were washed once with TNMFH medium and infected with AcMNPV-LacZGUS (MOI = 5). At 24 h p.i., the cell supernatants were collected and the virus titers were determined by TCID₅₀ assays.

2.8. Confocal microscopy and imaging

Sf9 cells were cultured on glass coverslips in 12-well plates, and were transfected with 2 µg of a plasmid expressing GFP, or GFP-tagged Rab4, Rab5, Rab7, or Rab11. At 16 h p.t., the cells were pre-chilled at 4 °C for 30 min and then incubated with the purified AcMNPV-3mC (MOI = 20) at 4 °C for 1 h. After removing the medium containing viruses, cells were washed twice with cold TNMFH medium and shifted to 27 °C for 15 and 30 min. At different time points, the infected cells were fixed with 3.7% paraformaldehyde in PBS (pH 7.4) for 10 min. After permeabilizing with 0.05% Triton X-100 in PBS (pH 7.4) for 1 min, the cell nuclei were stained with Hoechst 33,258 (1 µg/ml, Invitrogen). Images were collected on a Leica TCS SP8 confocal microscope (Leica Microsystems Inc.) with a 63 × oil immersion objective (NA 1.4). GFP and mCherry signals were collected separately from the Hoechst33258 signal and later superimposed. Colocalization of GFP-tagged Rab proteins and mCherry-labeled BVs was quantified using Fiji

image processing package (Schindelin et al., 2012).

2.9. Infectivity assay

Sf9 cells in 12-well plates were transfected with 2 μ g of a plasmid expressing GFP, or GFP-tagged WT or DN Rab4, Rab5, Rab7, or Rab11. At 16 h p.t., the cells were infected with AcMNPV-LacZGUS (MOI = 5). At 24 h p.i., cells and the supernatants were separately collected. Cell samples were analyzed for the expression of GFP-tagged Rab proteins by Western blotting and virus titers were measured by TCID₅₀ assays.

2.10. RNAi assav

The dsRNA-based RNAi assay was performed as described previously (Yue et al., 2018). A 495 bp fragment of *gfp* or a 311–452 bp fragment of the coding sequence of Sf9 *dynamin* and *rab* genes was amplified by using PCR with each primer containing the T7 promoter sequence (Table 1). PCR products were gel purified using QIAEXII Gel Extraction Kit (QIAGEN). The dsRNA were transcribed with the T7 RiboMAX™ Express RNAi System (Promega) and purified with RNeasy Mini Kit (QIAGEN).

Sf9 cells in 12-well plates were transfected with 7.5 μ g of dsRNA targeting *dynamin* or each *rab* gene, or 7.5 μ g of the *gfp* dsRNA as a negative control. At 48 h p.t., one set of the cells were used to assess the cell viability as described above, the other set of the cells were used to determine the gene knockdown efficiency by analyzing the transcripts of each target gene by qPCR. To determine the effects of RNAi on virus infection, Sf9 cells in 12-well plates were transfected with 7.5 μ g of dsRNA targeting *dynamin* or each of *rab* genes, or 7.5 μ g of the *gfp* dsRNA. At 48 h p.t., the cells were infected with AcMNPV-LacZGUS (MOI = 5). At 24 h p.i., virus titers were measured by TCID₅₀ assays.

2.11. Analysis of viral gene expression and DNA replication

Sf9 cells in 12-well plates were treated with 10 and 20 μ M dynasore for 3 h, or transfected with 2 µg of a plasmid expressing GFP or GFPtagged WT or DN Rab proteins. After removing the drug or at 16 h p.t., the cells were infected with AcMNPV-LacZGUS (MOI = 5). In each experiment, one set of the cells were collected and lysed with 1% Triton-X100 in PBS (pH7.4) at 6 and 24 h p.i. and used to measure the β-galactosidase (β-Gal) or β-glucuronidase (β-Gluc) activities by using the substrate Chlorophenol red-β-D-galactopyranoside (CPRG, Roche Diagnostics GmbH) or 4-Nitrophenyl β-D-glucuronide (PNPG, Sigma-Aldrich). Another set of the cells were collected at 24 h p.i. and total DNA was extracted using a DNeasy Blood & Tissue kit (QIAGEN). Viral genomic DNA was quantified by qPCR as described above. Each PCR mixture contained 10 μl SYBR® Premix ExTaq II (TaKaRa), 2.5 μM each primer (ODV-e56F and ODV-e56R) (Table 1), and 1 ng of the DNA template. A standard curve was generated by a serial dilution of ODVe56pGEM as described previously (Li and Blissard, 2012). AcMNPV genomic DNA was expressed as numbers of viral DNA copies per cell.

2.12. BVs binding and internalization

Sf9 cells in 12-well plates were incubated with TNMFH medium containing 10 or 20 μM dynasore for 3 h or transfected with 2 μg of each plasmid expressing GFP, or GFP-tagged WT or DN Rab5 and Rab11. After removing the drug, or at 16 h p.t., the cells were prechilled at 4 °C for 30 min and then incubated with the purified AcMNPV-LacZGUS (MOI = 5) at 4 °C for 1 h. After removing the virus inoculum, cells were washed twice with cold TNMFH medium. Then, one set of the cells were used to extract total DNA at 4 °C by using DNeasy Blood & Tissue kit (QIAGEN). Another set of the cells was shifted to 27 °C for 5, 15, and 30 min to allow virus internalization. At the different incubation time points at 27 °C, the cells were treated with citrate buffer (40 mM sodium citrate, 135 mM NaCl, and 10 mM KCl,

pH 3.1) for 1 min to inactivate and remove non-internalized viruses as described previously (Fan et al., 2017; Li et al., 2017) and then total DNA was extracted. Viral genomic DNA in total DNA extracts was quantified by qPCR.

2.13. Direct fusion assay

A direct fusion assay was performed as described previously (Dong et al., 2010) with minor modifications. Sf9 cells in 12-well plates were transfected with 2 μg of the plasmid GFP-pBlue, GFP-Rab5pBlue, GFP-Rab5S36N-GFPpBlue, GFP-Rab11pBlue, or GFP-Rab11S25NpBlue. At 16 h p.t., the cells were pre-chilled at 4 °C for 30 min and then incubated with AcMNPV-LacZ-GUS (MOI = 5) at 4 °C for 1 h. After removing the virus inoculum, cells were washed once with cold TNMFH medium and then treated with acidic TNMFH medium (pH 5.0) or normal TNMFH (pH 6.2) at 4 °C for 3 min. Then, the cells were washed once with cold TNMFH medium and shifted to 27 °C. At 6 h p.i., one set of the cells were lysed with 1% Triton-X100 in PBS (pH7.4) and the β -Gal activity was measured using the substrate CPRG. At 24 h p.i., the supernatant was collected from the other set of infected cells and virus titers were measured by $TCID_{50}$ assays.

2.14. Analysis of virus egress

Sf9 cells in 6-well plates were transfected with 4 μg of one of the following AcMNPV bacmid DNAs: GFP-Bac, GFP-Rab5-Bac, GFP-Rab5-Bac, GFP-Rab11-Bac, or GFP-Rab11 $^{\rm S25N}$ -Bac, which express GFP or GFP-tagged WT or DN Rab5 and Rab11, respectively. At 24 h p.t., one set of the cells were counted under epifluorescence microscopy (Nikon Eclipse Ti) to evaluate the transfection efficiency. The other set of the cells were collected and lysed as above and the β -Gluc activity was determined. Supernatants were also collected and virus titers were determined by TCID $_{50}$ assays.

2.15. Western blot analysis

The transfected-infected cells were lysed in Triton X-100 lysis buffer (150 mM NaCl, 0.1% Triton X-100, 50 mM Tris, pH 8.0) containing the complete protease inhibitor cocktail (Roche Applied Science) and analyzed by 10% SDS-polyacrylamide gels. After transferring the protein samples to polyvinylidene difluoride (PVDF) membrane (0.45 μm , Millipore), GFP and GFP-tagged proteins were detected with an anti-GFP polyclonal antibody (GenScript), alkaline phosphatase-conjugated anti-rabbit IgG, and nitroblue tetrazolium/5-bromo-4-chloro-3-in-dolylphosphate (NBT/BCIP, Promega).

3. Results

3.1. Changes in dynamin and rab transcript levels following AcMNPV infection

Comparative analysis of genome sequences indicates that dynamin, Rab4, Rab5, Rab7, and Rab11 are conserved in sequenced insect genomes. Compared with mammalian genomes, where these proteins-encoding genes are typically expanded into multiple isoforms (Klopper et al., 2012), only a single ortholog for each protein-encoding gene was found in representative insect genomes (Table 2). To determine the transcript levels of *dynamin* and *rab* genes (*rab4*, *rab5*, *rab7*, and *rab11*) in AcMNPV-infected Sf9 cells, we cloned cDNAs of these genes, and used qPCR to measure transcript levels of the genes from uninfected and AcMNPV-infected Sf9 cells at various times post infection. As shown in Fig. 1, AcMNPV infection significantly up-regulated the transcript levels of *dynamin*, *rab5*, and *rab11* at 1–3 h p.i. By 6 h p.i., the transcript levels of *dynamin* had returned to near or slightly below control levels and decreased thereafter. The transcript levels of *rab5* and *rab11* remained at increased levels through 6 h p.i., but decreased after

Table 2Dynamin and Rab proteins in yeast, mammals, and insects.

Protein	Main localization and function in	Species		
	endocytic trafficking	Yeast ^a	Mammals	Insects ^b
dynamin	Endocytic pits, membrane fission	Vps1	dynamin 1 dynamin 2 dynamin 3	dynamin
Rab4	Early endosomes, endocytic recycling	Ypt4	Rab4A Rab4B	Rab4
Rab5	Clathrin-coated vesicles and early endosomes, endocytic internalization and early endosome fusion and biogenesis	Ypt51 Ypt10	Rab5A Rab5B Rab5C	Rab5
Rab7	Late endosomes, late endocytic trafficking	Ypt7	Rab7A Rab7B	Rab7
Rab11	Recycling endosomes, endocytic recycling	Ypt31 Ypt32	Rab11A Rab11B	Rab11

Note.

- ^a Yeast represents Saccharomycotina.
- b Insects represent sequenced insect genomes from 6 Orders, including Coleoptera (*Tribolium castaneum*, http://beetlebase.org), Diptera (*Aedes aegypti*, *Anopheles gambiae*, *Culex quinquefasciatus*, *Drosophila melanogaster*, http://flybase.org and http://www.vectorbase.org), Hemiptera (*Acyrthosiphon pisum*, http://www. aphidbase.com), Hymenoptera (*Apis mellifera*, *Harpegnathos saltator*, *Nasonia vitripennis*, http://hymenopteragenome.org), Lepidoptera (*Bombyx mori*, *Danaus plexippus*, http://silkworm.genomics.org.cn and http://monarchbase.umassmed.edu) and Phthiraptera (*Pediculus humanus corporis*, http://www.vectorbase.org).

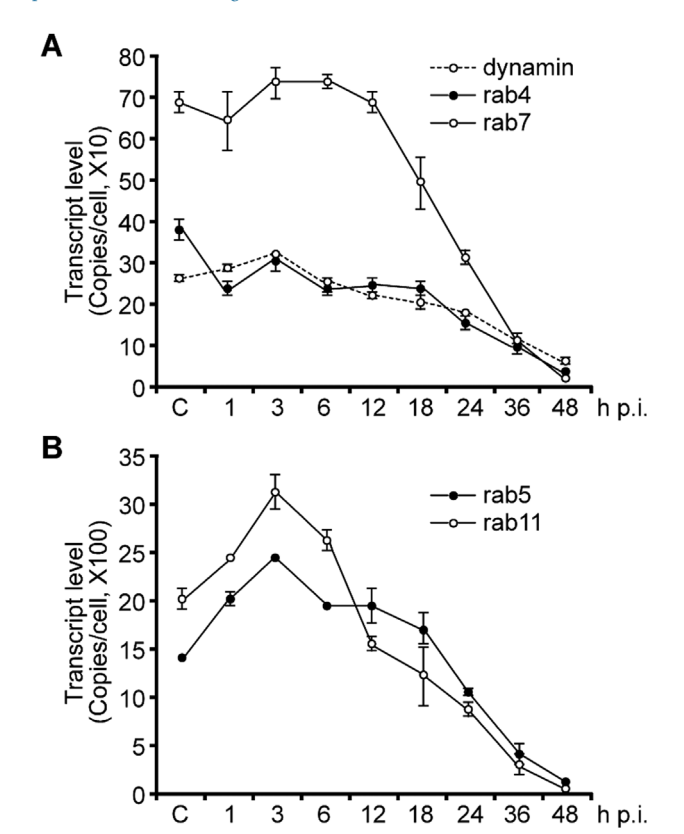


Fig. 1. Transcript profiles of *dynamin* and *rab* genes in AcMNPV-infected cells. Transcript levels of *dynamin*, *rab4*, *rab5*, *rab7*, and *rab11* in mock-infected (C, control) or AcMNPV-infected Sf9 cells at various time points (1–48 h) p.i. were measured by qPCR. The cells were infected at the same time and the mock-infected cells were collected at 1 h p.i. Error bars represent standard deviations (SD) from the mean of three replicates.

12 h p.i. or 6 h p.i., respectively (Fig. 1 A, B). Compared with transcripts for *rab5* and *rab11* genes, the transcript levels of *rab4* were significantly reduced after virus inoculation, whereas that of *rab7* appeared to be unaffected by viral infection through 12 h p.i., after which, transcript levels decreased (Fig. 1 A). Overall, the transcript level changes for *dynamin* and *rab* genes in Sf9 cells were similar to those of transcriptome data observed in AcMNPV-infected *Trichoplusia ni* cells (Tnms42) (Chen et al., 2014), suggesting that cellular dynamin, Rab5, and Rab11 may play important roles in AcMNPV infection.

3.2. Dynamin is required for infectious AcMNPV production

To determine whether dynamin is involved in AcMNPV propagation, we initially examined the effects of dynasore (a reversible specific inhibitor of dynamin) (Macia et al., 2006) on infectious AcMNPV production. General effects of dynasore on the proliferation of Sf9 cells were evaluated by measuring the viability of cells treated with 5–50 μM dynasore. As shown in Fig. S1A, the viability of Sf9 cells treated with 5–25 μM dynasore was similar to that of the control (DMSO-treated cells), but 50 μM dynasore reduced the viability to approximately 70%. Thus, dynasore treatment at concentrations $\leq 25~\mu M$ did not appear to have a negative effect on the viability of Sf9 cells.

To determine whether dynamin was required for productive AcMNPV infection, we pre-treated Sf9 cells with 5–25 μ M dynasore then infected the cells with AcMNPV-3mC. At 24 h p.i., the numbers of infected cells were slightly decreased in cells treated with 5 or 10 μ M dynasore (Fig. 2A), and the infectious virus production in both treatments was reduced about 2.0 fold (Fig. 2B). At slightly higher concentrations of dynasore (15–25 μ M) we observed substantially lower numbers of infected cells (Fig. 2A), and infectious virus titers were

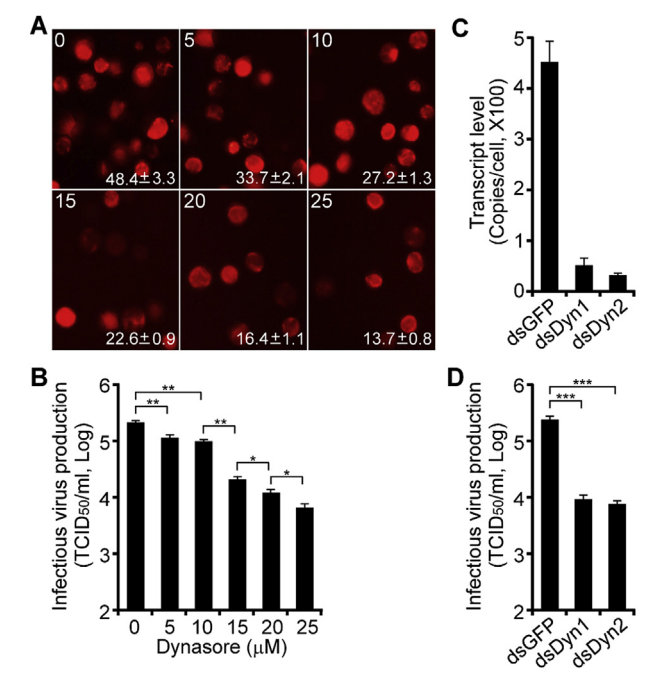


Fig. 2. Effects of inhibition of dynamin on infectious AcMNPV production. (A, B) Sf9 cells were pre-treated with dynasore (5–25 μM) for 3 h. After removing the drug, the cells were infected with AcMNPV-3mC. At 24 h p.i., the cells were visualized by epifluorescence microscopy (A) and infectious virus production was measured by $TCID_{50}$ assays (B). (C, D) Sf9 cells were transfected with a dsRNA specific for *dynamin* (dsDyn1 or dsDyn2) or *gfp*. At 48 h p.t., one set of the cells was collected and *dynamin* transcript levels were quantified by qPCR (C), and another set of the cells were infected with AcMNPV-LacZGUS. At 24 h p.i., infectious virus titers were determined by $TCID_{50}$ assays (D). Error bars represent SD from the mean of three replicates. *, P < 0.005; **, P < 0.005; ***, P < 0.0005 (by paired two-tailed t-test).

reduced by 10.1, 15.9, and 28.3 fold in cells treated with 15, 20 and 25 μM dynasore, respectively (Fig. 2B).

To further examine the effects of dynamin on infectious AcMNPV BVs production, we used RNAi to knockdown dynamin. Sf9 cells were transfected with either dsRNAs that target Sf9 dynamin (dsDyn1 and dsDyn2), or dsRNA targeting gfp as a control. RNAi knockdown efficiencies were approximately 90% (Fig. 2C) as determined by qPCR. Transfection with dsRNA targeting dynamin or gfp resulted in no significant change in the viability of Sf9 cells at 48 h p.t. (Fig. S1C). RNAi knockdowns of dynamin resulted in a significant reduction in the production of infectious AcMNPV (Fig. 2D), similar to the result observed from treatments with dynasore. Together, these results indicate that functional dynamin was required for the efficient production of infectious AcMNPV.

3.3. Entry of budded virions of AcMNPV is dependent on dynamin

To examine the possibility that the negative effects resulting from dynamin inhibition or knockdown might result from early events in the infection cycle, Sf9 cells were pre-treated with 10 and 20 μM dynasore for 3 h and then infected with AcMNPV-LacZGUS that contains LacZ and GUS reporter genes, under the control of the AcMNPV ie1 early/late promoter and p6.9 late promoter, respectively. At early (6 h p.i.) and later (24 h p.i.) infection times, relative activities of β -Gal and β -Gluc were significantly reduced when compared with the controls, and the reduction of enzyme activity in both cases was dependent on the

concentration of dynasore (Fig. 3A and B). In addition, inhibition of dynamin with dynasore also resulted in significantly reduced levels of viral genomic DNA at 24 h p.i. (Fig. 3C). Because early and late gene expression and viral DNA accumulation were all reduced, these results suggest that disrupting dynamin activity inhibits viral infection at a step prior to early gene expression, possibly inhibiting virions binding or entry.

To determine whether the reduced virus production in the presence of dynasore may have resulted from a reduction in virus binding, we analyzed the cell binding efficiency of BVs in cells pre-treated with dynasore. AcMNPV-LacZGUS was incubated with Sf9 cells at 4 °C. At 4 °C, virions can bind to cells but they are not internalized (Zhou and Blissard, 2008). After removing unbound virus and washing cells at 4 °C, cells were collected and viral genomic DNA was quantified by qPCR. Cells pretreated with dynasore (10 or 20 μ M) showed similar levels of viral genomic DNA, as compared with control DMSO-treated cells (Fig. 3D), suggesting that dyansore treatment did not affect virion binding.

To next examine whether inhibiting dynamin activity affects virus entry, virion internalization was quantified. Sf9 cells were pre-treated with dynasore then incubated with the virus at 4 °C to permit binding. The virus inoculum was then removed and the temperature was raised to 27 °C for 5–30 min to allow the virus to enter cells. Any virions remaining at the cell surface were inactivated and removed by treatment with citrate buffer (pH 3.1). Total DNA was then extracted and viral genomic DNA was quantified by qPCR. It is noting that, although

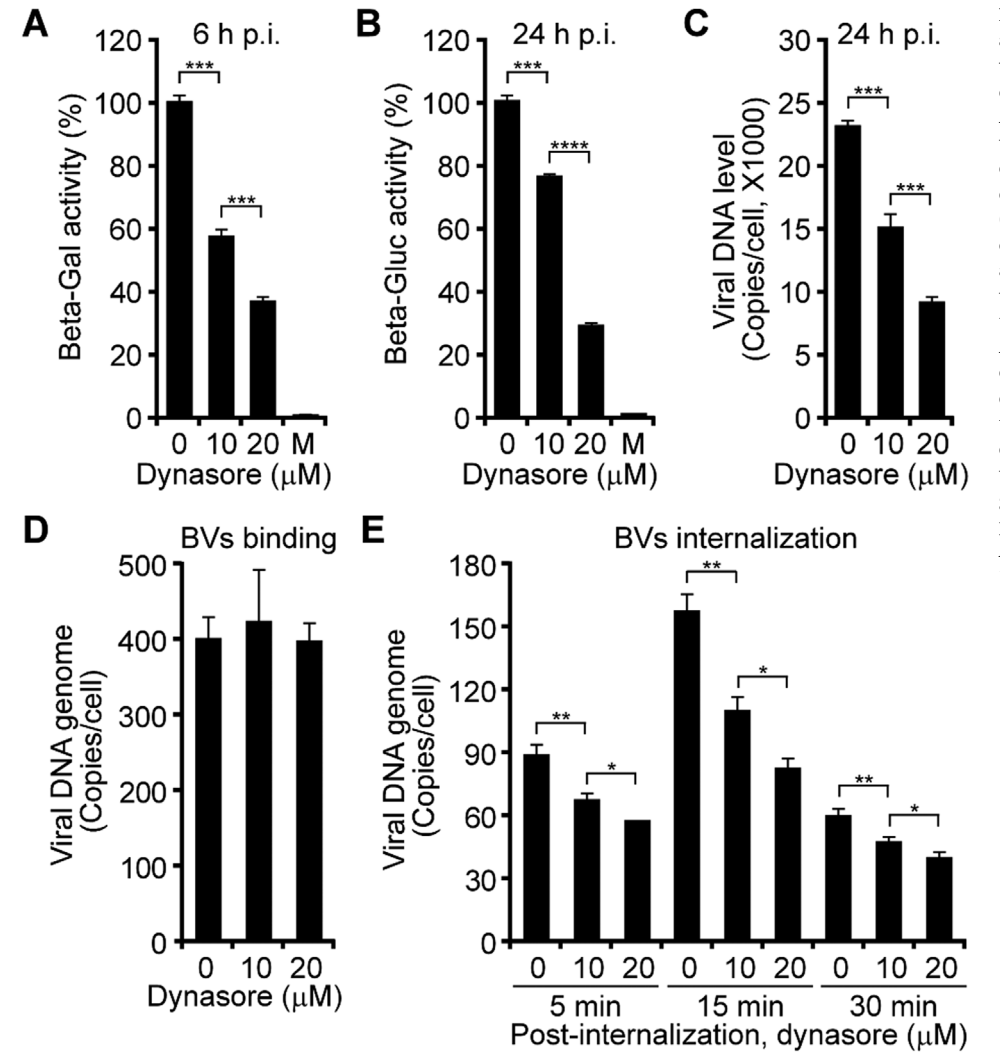


Fig. 3. Effects of dynamin inhibition on early and late events of AcMNPV infection and virus binding and internalization. (A-C) Sf9 cells were pre-treated with dynasore for 3 h. After removing the drug, cells were infected with AcMNPV-LacZGUS. At 6 and 24 h p.i., the cells were lysed and the early and late viral gene expression was monitored by analyzing Beta-Gal (A) and Beta-Gluc activities (B). Accumulation of viral genomic DNA was determined by qPCR at 24 h p.i. (C). (D, E) Sf9 cells were pre-treated with dynasore for 3 h. After removing the drug, the cells were incubated with the purified AcMNPV-LacZGUS at 4 °C for 1 h. One set of the cells were lysed and virus binding efficiency was determined by measuring viral genomic DNA using qPCR (D). The other set of the cells were cultured at 27 °C for 5-30 min, internalized viruses were determined by measuring the viral genomic DNA using qPCR (E). Error bars represent SD from the mean of three replicates. *, P < 0.05; **, P < 0.005. ***, P < 0.0005,****, P < 0.00005 (by paired two-tailed *t*-test).

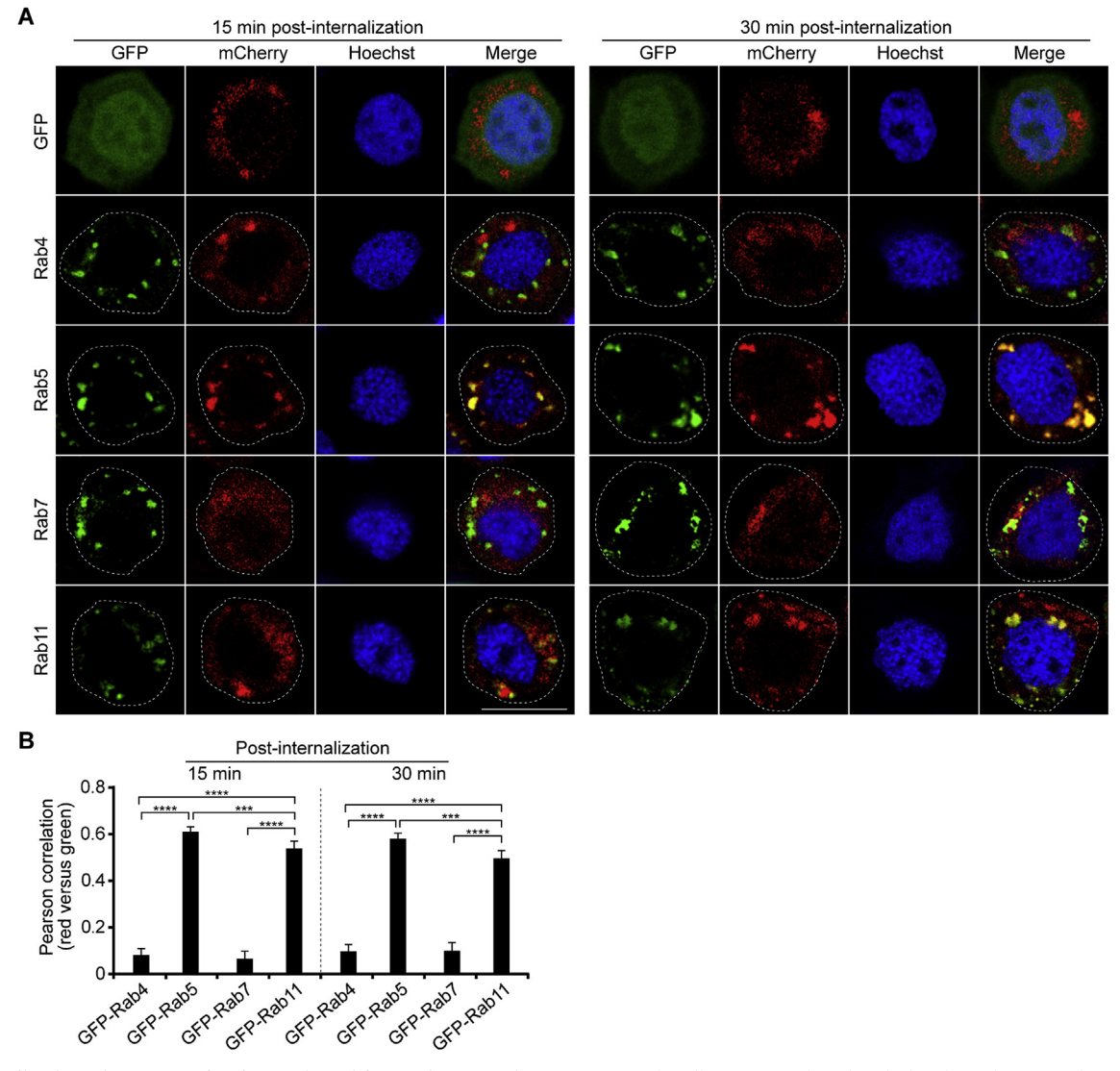


Fig. 4. Colocalization of GFP-tagged Rab proteins with entering BVs of AcMNPV. (A) Sf9 cells were transfected with the plasmids separately expressing GFP-tagged Rab proteins. At 16 h p.t., the cells were infected with AcMNPV-3mC at 4 °C for 1 h, then the cells were incubated at 27 °C for 15 and 30 min and analyzed by confocal microscopy. Cell boundaries were traced with circled dash lines. Scale bar, 10 μ m. (B) Colocalization between GFP-tagged Rab proteins and mCherry-labeled AcMNPV was quantified by measuring the Pearson's correlation coefficient for red and green pixels in each cell. Totally, 30 cells were calculated for each construct. *****, P < 0.00001 (by paired two-tailed t-test). (For interpretation of the references to colour in this figure legend, the reader is referred to the Web version of this article.)

acidic Grace's medium (pH 4.8) can trigger the fusion of AcMNPV BVs with the plasma membrane and induce internalization of viruses into Sf9 cells (Dong et al., 2010), the citrate buffer (pH 3.1) treatment could efficiently inactivate and remove cell surface-bound BVs as previously described for other viruses (Fan et al., 2017; Li et al., 2017) (Fig. S2). As shown in Fig. 3D and E, prior dynasore treatment of the cells had no substantial effect on BVs binding but significantly reduced the amount of viral DNA detected after binding and 5–30 min incubation at 27 °C. Combined, these data indicate that while dynamin appears to play little or no role in virion binding, dynamin activity was important for efficient virion internalization.

3.4. Entering virions colocalize mainly with Rab5 and Rab11

During endocytosis, trafficking of endocytic vesicles is regulated by a variety of Rab proteins. To examine the roles and associations of Rab4, Rab5, Rab7, and Rab11 in AcMNPV-infected Sf9 cells, we used confocal microscopy to examine the localization of internalized BVs in relation to these cellular Rab proteins. In Sf9 cells transiently expressing

GFP-tagged Rab proteins, internalized mCherry-labeled BVs colocalized mainly with GFP-Rab5 and GFP-Rab11 at 15 and 30 min post-internalization (Fig. 4; Rab5 and Rab11). In contrast, only a minor colocalization was observed between entering BVs and GFP-Rab4 or GFP-Rab7 (Fig. 4, Rab4 and Rab7). Thus, colocalization results suggest that during trafficking of internalized BVs, they appear to be associated with Rab5 and Rab11.

3.5. Rab5 and Rab11 are required for efficient production of infectious AcMNPV

To identify requirements of Rab proteins for productive virus infection, we first made DN constructs of Rab4, Rab5, Rab7, and Rab11 (GFP-Rab4^{N121I}, GFP-Rab5^{S36N}, GFP-Rab7^{T22N}, and GFP-Rab11^{S25N}). These point mutations were previously shown to restrict Rab proteins to the inactivated GDP-bound state (Buczynski et al., 1997; Cormont et al., 1996; Stenmark et al., 1994; Ullrich et al., 1996). We analyzed the effect of expressing each DN Rab protein on production of infectious AcMNPV. For this assay, Sf9 cells were transfected with the plasmid

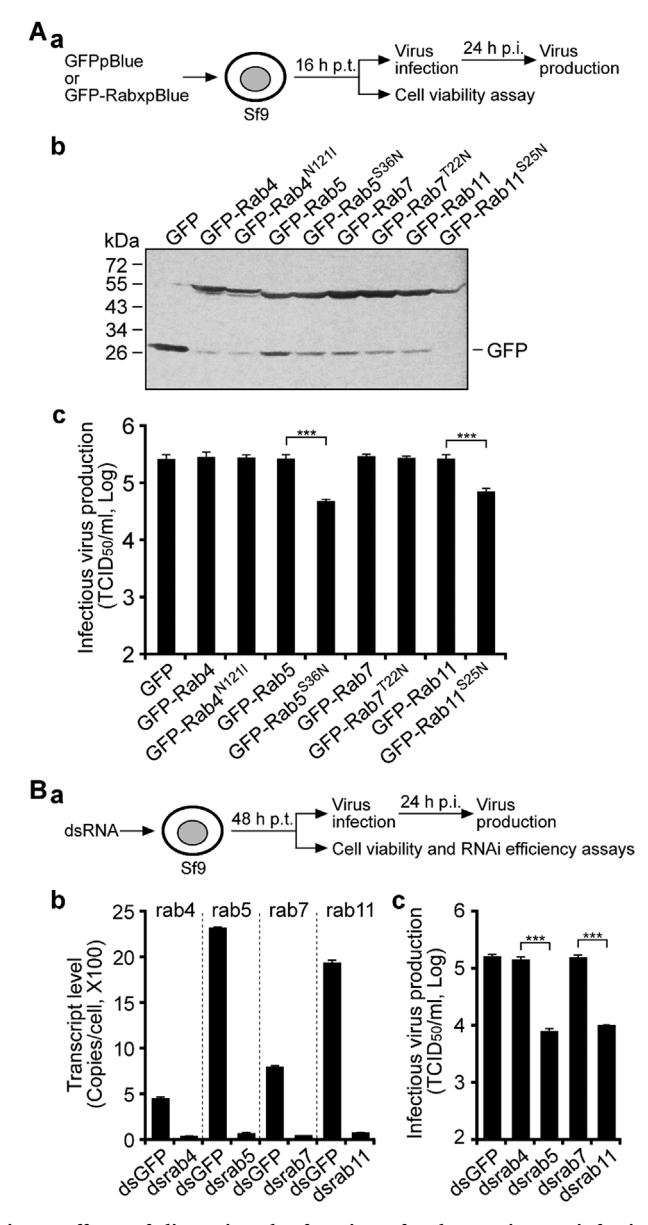


Fig. 5. Effects of disrupting the function of Rab proteins on infectious AcMNPV production. (A) Effects of DN Rab protein expression on infectious AcMNPV production. (a) Schematic representation of the viral infection assay. Sf9 cells were transfected with the plasmids separately expressing GFP or GFPtagged WT or DN Rab proteins. At 16 h p.t., one set of the cells were used to determine the cell viability (Fig. S1B), and another set of the cells were infected with AcMNPV-LacZGUS. At 24 h p.i., the expression of GFP-tagged Rab proteins was analyzed by Western blotting (b), the titers of infectious BVs were determined by TCID₅₀ assays (c). (B) Effects of Rab-targeted RNAi knockdowns on infectious AcMNPV production. (a) Schematic representation of the RNAi assay. (b, c) Sf9 cells were transfected with the dsRNAs targeting rab genes or the control gfp. At 48 h p.t., one set of the cells was lysed and the transcript level of each rab gene was quantified by qPCR (b), and another set of the cells was infected with AcMNPV-LacZGUS. At 24 h p.i., infectious virus titers were determined by TCID50 assays (c). Error bars represent SD from the mean of three replicates. ***, P < 0.0005 (by paired two-tailed t-test).

expressing a GFP-tagged WT or DN Rab protein (or a GFP control). At 16 h p.t., the viability of the transfected cells was measured and the cells were infected with AcMNPV-LacZGUS. At 24 h p.i., the infectious virus titers were determined (Fig. 5A, panel a). When compared with the control (cells expressing GFP), transient expression of the GFP-tagged WT or DN Rab proteins has no significant effect on the viability of Sf9 cells (Fig. S1B). Western blot analysis indicated that each of the

GFP-tagged Rab constructs were expressed at similar levels in transfected-infected cells (Fig. 5A, panel b). The production of infectious AcMNPV was significantly reduced in the presence of DN Rab5 and DN Rab11, with reductions of approximately 73–82% (Fig. 5A, panel c). In contrast, expression of DN Rab4 and Rab7 had no notable effect on infectious virus production compared with that in Sf9 cells expressing the GFP or GFP-Rab control (Fig. 5A, panel c).

To confirm these observations, we also used RNAi to examine the effects of *rab* gene knockdowns on the production of infectious AcMNPV. Sf9 cells were transfected with a dsRNA specific for each of *rab* genes (*rab4*, *rab5*, *rab7*, and *rab11*) or a dsRNA targeting a *gfp* control gene (Fig. 5B, panel a). Knockdown efficiencies were monitored by qPCR and *rab* transcript levels were decreased by approximately 90–95% in comparison with the *gfp* dsRNA control at 48 h p.t. (Fig. 5B, panel b). Transfection with the dsRNA targeting *rab* genes or *gfp* resulted in no significant change in the viability of Sf9 cells at 48 h p.t. (Fig. S1C). We found that RNAi mediated depletion *rab5* and *rab1*1 mRNA resulted in a dramatic reduction (approximately 15 fold) in the production of infectious AcMNPV (Fig. 5B, panel c). Thus using both DN Rab proteins and RNAi knockdowns, these results suggest that Rab5 and Rab11 are important for the efficient production of infectious AcMNPV BVs.

3.6. Rab5 and Rab11 are necessary for internalization of budded virions

Since entering BVs were observed to colocalize mainly with Rab5 and Rab11 (Fig. 4), the negative effects of perturbing Rab5 and Rab11 on infectious BVs production may be related to effects on virus entry. To examine this possibility, Sf9 cells were transfected with the plasmids expressing GFP-tagged Rab (WT or DN Rab5 or Rab11) or GFP. At 16 h p.t., the cells were infected with the virus AcMNPV-LacZGUS (Fig. 6A, panel a). At 6 h and 24 h p.i., the relative activities of β -Gal and β -Gluc were significantly reduced in cells expressing DN Rab5 and DN Rab11 (Fig. 6A, panels b and c). We also analyzed viral genomic DNA accumulation at 24 h p.i. using qPCR. Consistent with the reporter gene expression data, viral genomic DNA levels were substantially lower in cells expressing DN Rab5 and Rab11 (Fig. 6A, panel d). As early and late gene expression and viral DNA production were all reduced by DN Rab5 and Rab11, these results suggest an effect of Rab5 and Rab11 on virus binding, internalization, or trafficking.

We first examined AcMNPV BVs binding to cells expressing DN Rab5 or Rab11. Sf9 cells were transfected with a plasmid expressing GFP-tagged WT or DN forms of Rab5 or Rab11. At 16 h p.t., the cells were incubated with AcMNPV-LacZGUS at 4 °C. After removing unbound virus, viral genomic DNA was measured by qPCR (Fig. 6B, panel a). We observed no significant reduction in viral DNA detected from cells expressing GFP-Rab5^{S36N} or GFP-Rab11^{S25N}, when compared with cells expressing control GFP or GFP-tagged WT Rab5 and Rab11 proteins (Fig. 6B, panel b). Thus, virion binding appeared to be unaffected by these DN Rab proteins. To examine possible effects of DN Rab5 and Rab11 on virion internalization, internalized BVs were similarly quantified by qPCR. For these experiments, Sf9 cells were transfected with the plasmid expressing one of the Rab constructs. At 16 h p.t., cells were incubated with the virus at 4 °C to permit virus binding. After removing the virus inoculum, the culture temperature was raised to 27 °C for 5–30 min to allow the virus to enter cells (Fig. 6B, panel a). Then, the non-internalized virions were inactivated and removed (by treatment of cells with citrate buffer, pH 3.1), and total DNA was extracted and viral genomic DNA was quantified. The expression of control GFP-tagged WT Rab5 and Rab11 did not affect the internalization of BVs (Fig. 6B, panel c). However, expression of DN Rab5 and Rab11 resulted in significantly lower quantities of viral DNA detected following the 5-30 min BVs internalization period. Together, these results suggest that the efficient internalization of AcMNPV BVs is dependent on functional Rab5 and Rab11.

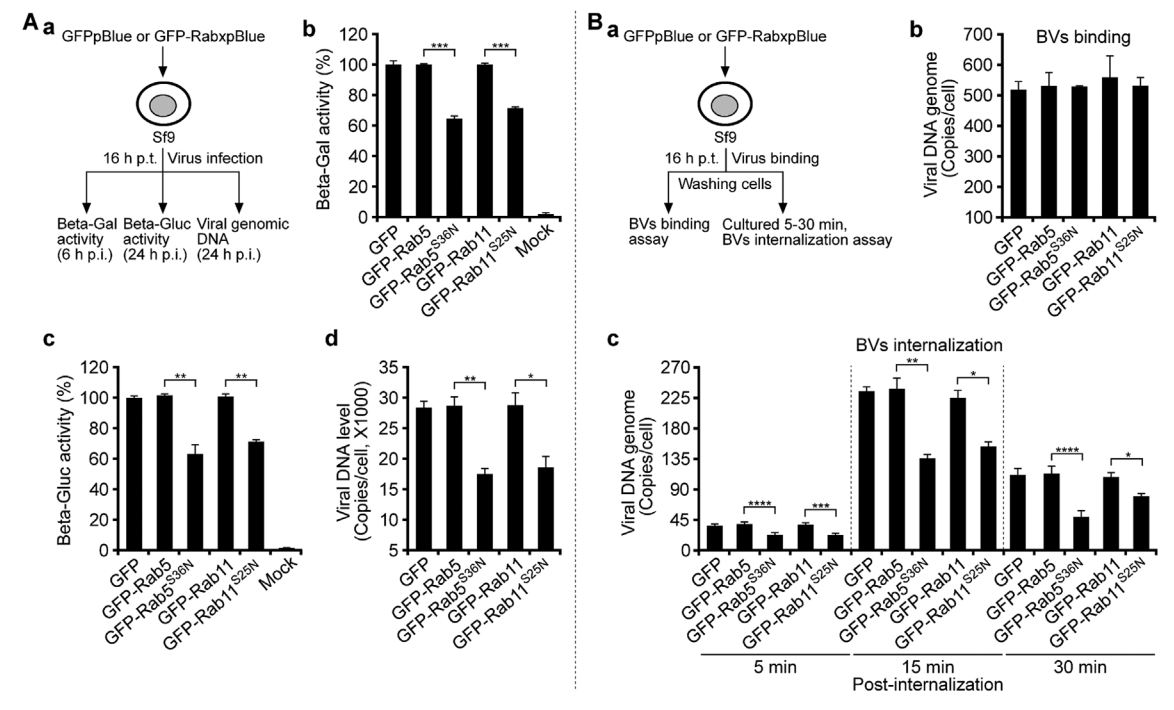


Fig. 6. Effects of DN Rab5 and Rab11 on early and late steps of virus infection (A) and BVs binding and internalization (B). (A) (a) Schematic representation of the viral infection assay. Sf9 cells were transfected with the plasmids expressing GFP or GFP-tagged WT or DN Rab5 or Rab11. At 16 h p.t., the cells were infected with AcMNPV-LacZGUS. At 6 and 24 h p.i., the cells were lysed and used to measure Beta-Gal (b) and Beta-Gluc activities (c). Accumulation of viral genomic DNA was measured at 24 h p.i. by qPCR (d). (B) (a) Schematic representation of BVs binding and internalization assays. Sf9 cells were transfected with a plasmid expressing GFP or GFP-tagged WT or DN Rab5 or Rab11. At 16 h p.t., the cells were infected with the purified AcMNPV-LacZGUS at 4 °C for 1 h. Then, one set of the cells was lysed and virus binding efficiency was determined by measuring viral genomic DNA using qPCR (b). The other set of cells was cultured at 27 °C for 5–30 min and then the internalized BVs were measured by qPCR of viral genomic DNA (c). Error bars represent SD from the mean of three replicates. *, P < 0.005; **, P < 0.0005; ***, P < 0.00

3.7. Is Rab5 or Rab11 required for AcMNPV BVs egress?

As described above, DN Rab5 and DN Rab11 had substantial negative effects on virion entry. Next, we examined the possible roles of Rab5 and Rab11 in virion budding and/or release. For these studies, we circumvented effects on viral entry by initiating viral infection by either a) low-pH triggered direct fusion of BVs at the cell surface, or b) directly transfecting Sf9 cells with viral genomic DNA. Prior studies demonstrated that low-pH triggered direct-fusion of the AcMNPV BVs envelope with the cellular plasma membrane can efficiently mediate entry of viral nucleocapsids into Sf9 cells, in an endosome-independent manner (Dong et al., 2010). Following the initiation of infection by fusion at the cell surface, we analyzed infectious BVs production over a narrow time period following virus infection (24 h p.i.). For these experiments, Sf9 cells were transfected with a plasmid expressing GFP or GFP-tagged WT or DN Rab5 or DN Rab11. At 16 h p.t., the cells were infected with AcMNPV-LacZGUS. After binding at 4 °C, virus entry was either allowed to proceed normally (cells were maintained at pH 6.2), or entry was triggered at the cell surface by low pH treatment (pH 5.0) at 4 °C. One set of the cells were lysed at 6 h p.i. and successful viral entry was assessed by measuring relative activities of β-Gal (Fig. 7A, panel a). As shown in Fig. 7A (panel b, pH 6.2), the presence of DN Rab5 or Rab11 significantly reduced the expression of β-Gal in cells infected under normal conditions (pH 6.2). However, when infection was initiated by virion fusion at the cell surface (pH 5.0), the activities of β -Gal in cells expressing DN Rab5 or Rab11 were similar to those of cells expressing WT Rab5 or Rab11, or GFP (Fig. 7A, panel b, pH 5.0). The expression of DN Rab5 or Rab11 also significantly reduced the amounts of infectious AcMNPV BVs in supernatants from cells infected under normal conditions (Fig. 7A, panel c, pH 6.2). However, when infection was initiated by low-pH triggered cell surface entry, BVs production was not affected by the presence of DN Rab5 or Rab11

(Fig. 7A, panel c, pH 5.0). These results suggest that the functional roles of Rab5 and Rab11 in AcMNPV infections are associated primarily with virus entry and not substantially with virus egress.

In a second set of experiments, we transfected Sf9 cells with AcMNPV bacmids encoding GFP or GFP-tagged WT or DN Rab5 or Rab11 under the early/late promoter of ie1. Bacmids also encoded a reporter gene (GUS) under a late promoter (p6.9). Infectious BVs production was determined at 24 h p.t. (Fig. 7B, panel a). At 24 h p.t., GFP fluorescence measurements showed that transfection efficiencies and initiation of infection by the different bacmids were equivalent (app. 32–34% transfection efficiency, data not shown). The β -Gluc activities from cells transfected with different bacmids were also similar (Fig. 7B, panel b) confirming that transfection efficiencies were similar for all bacmid constructs, and that infection progressed into the late phase of the infection cycle. We found that production of infectious AcMNPV from cells transfected with bacmids expressing DN Rab5 or Rab11 was similar to that from cells expressing WT Rab5 or Rab11, or GFP (Fig. 7B, panel c). Thus, when entry effects were circumvented by each of the above approaches, we found no substantial effect of DN Rab5 or Rab11 expression on BVs production, suggesting that Rab5 and Rab11 play roles primarily in virion entry, and they may not play a substantial role in egress of AcMNPV BVs.

4. Discussion

In the early stages of infection by AcMNPV, the transcript levels of many host cellular genes involved in endosomal trafficking are upregulated (Chen et al., 2014) (Fig. 1). However, the precise trafficking routes of internalized BVs within endosomal compartments and the requirements for cellular factors that regulate endosomal trafficking are poorly understood. In the current study of AcMNPV infection of Sf9 cells, we found that efficient entry but not egress of BVs required

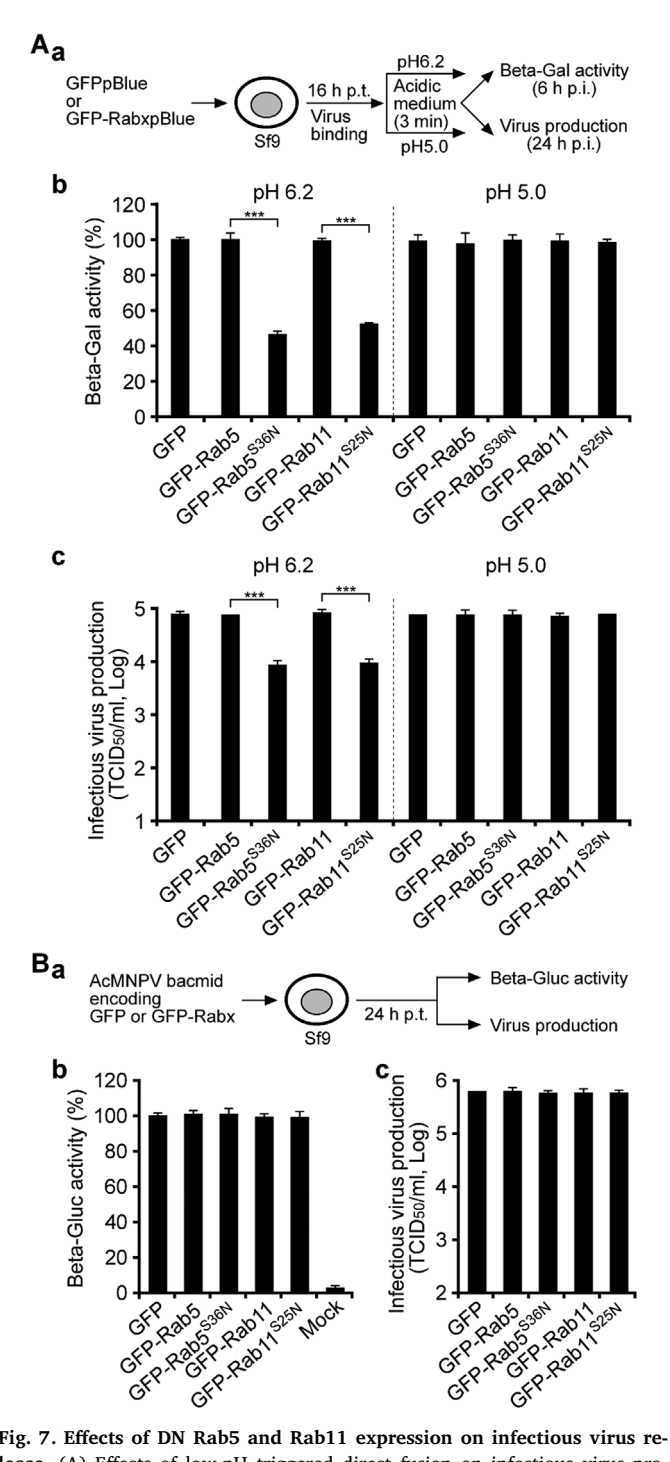


Fig. 7. Effects of DN Rab5 and Rab11 expression on infectious virus release. (A) Effects of low-pH triggered direct fusion on infectious virus production in cells expressing DN Rab5 and Rab11. (a) Schematic representation of the low-pH triggered direct fusion assay. Sf9 cells were transfected with the plasmid expressing GFP-tagged WT or DN Rab5 or Rab11. At 16 h p.t., the cells were infected with AcMNPV-LacZGUS at 4 °C for 1 h. After removing the viral inoculum, the cells were incubated with acidic TNMFH (pH 5.0) or normal TNMFH (pH 6.2) for 3 min. At 6 h p.i., one set of the cells were lysed and the early viral gene expression was monitored indirectly by analyzing Beta-Gal activities (b). At 24 h p.i., infectious virus titers were determined by TCID₅₀ assays (c). (B) Effects of bacmid transfection-mediated infection on infectious virus production in cells expressing DN Rab5 and Rab11. (a) Schematic representation of the transfection-infection assay. Sf9 cells were transfected with AcMNPV bacmid DNA expressing either GFP or GFP-tagged WT or DN Rab5 or Rab11. At 24 h p.t., late phase gene expression was monitored by analysis of the activity of Beta-Gluc (b). Infectious BVs production was measured at 24 h p.t. by a TCID50 assay (c). Error bars represent SD from the mean of three replicates. ***, P < 0.0005 (by paired two-tailed *t*-test).

functional dynamin, Rab5 and Rab11, but not Rab4 and Rab7. These results suggest that while trafficking through the cellular endosomal system during entry, internalized BVs are transported via early, maturing, and recycling endosomes.

Prior studies using chemical inhibitors of endosomal acidification or endosomal trafficking have concluded that AcMNPV BVs enter host cells by clathrin-mediated endocytosis (Hefferon et al., 1999; Long et al., 2006; Volkman and Goldsmith, 1985). In the current study, we analyzed the role of cellular dynamin on BVs entry. In canonical clathrin-mediated endocytosis, dynamin is responsible for constricting clathrin-coated pits and catalyzing the release of vesicles from the plasma membrane (Antonny et al., 2016). We found that disrupting the activity of dynamin with dynasore or with dsRNAs targeting dynamin, significantly reduced infectious BVs production and that overall negative effect on virus infection appears to be directly related to low efficiency entry of BVs into cells (Figs. 2 and 3).

In eukaryotic cells, Rab proteins are associated with the distinct intracellular compartments/organelles and function as molecular switches to tightly controls intracellular vesicle trafficking (Goody et al., 2017). During a short period following internalization from the cell surface, we observed the colocalization of the entering AcMNPV BVs with GFP-tagged Rab5 and Rab11 (Fig. 4). Expression of DN Rab5, and Rab5-targeted RNAi significantly reduced BVs internalization and AcMNPV infection (Figs. 5 and 6), suggesting that EE is a critical intracellular compartment for virus entry and productive infection. Rab5, which is used as a marker for EE, is involved in mediating transport of incoming vesicles to the EE and maturing endosomes (Huotari and Helenius, 2011). Rab5 coordinates with its effectors Rabex5 and Rabaptin5, the tethering factor EEA1, and the SNARE protein syntaxin 13, to regulate the fusion of vesicles with EE (Kummel and Ungermann, 2014). NSF, an AAA ATPase that is responsible for disassembly and recycling the SNARE complex (Zhao and Brunger, 2016), is necessary for Rab5 effectors and syntaxin 13 interactions (Kummel and Ungermann, 2014). Within EE, the ESCRT complex is involved in sorting cargos and segregating them into intraluminal vesicles (ILVs) to promote endosome maturation (Wollert and Hurley, 2010). The negative effect of perturbing the activity of Rab5 on AcMNPV infection could result from inhibiting either the delivery of incoming virions to EE or the internalization and sorting of virions into maturing endosomes. Consistent with this, RNAi or expression of DN constructs of ESCRT components and NSF also dramatically reduced the entry of BVs of AcMNPV into host cells (Guo et al., 2017; Li and Blissard, 2012; Yue et al., 2018).

The endosome system is a dynamic continuum, with cargos of EE translocated to maturing endosomes, LE, and RE through tight regulation (Huotari and Helenius, 2011). The EE compartment is critical for AcMNPV infection, but may not be the only site for releasing nucleocapsids into cytosol. Disruption of Rab5 function impairs the integrity of EE and affects endosomal maturation, which in turn may impact trafficking of virions to other endosomal compartments. Therefore, we also examined several other Rab proteins that regulate cargo delivery away from EE. Rab7 is localized to LE and is reported to function as a master regulator to control late endocytic trafficking from maturing endosomes to LE and lysosomes (Buczynski et al., 1997; Huotari and Helenius, 2011). Expression of DN Rab7^{T22N} or RNAi knockdown of Rab7 transcripts in Sf9 cells had no notable effect on infectious AcMNPV production in our analysis (Fig. 5) and we observed only a minor colocalization of internalized virions with GFP-tagged Rab7 (Fig. 4), suggesting that infection of AcMNPV may not require transport of internalized virions to LE to facilitate productive infection in Sf9 cells. Our data are consistent with a recent study of single-particle tracking, which indicated that nucleocapsids of AcMNPV BVs were released by membrane fusion in EE in Sf9 cells (Qin et al., 2019).

There appear to be two pathways for directing or recycling the internalized cargos of EE back to the cell surface. One more rapid pathway involves Rab4-regulated cargo recycling of EE directly to the

plasma membrane. Another involves Rab11 regulated cargo trafficking more slowly through RE (Huotari and Helenius, 2011). Using either DN Rab4^{N121I} expression or Rab4-targeted RNAi in Sf9 cells, we observed no substantial effect on infectious AcMNPV production (Fig. 5). This suggests that the Rab4-dependent recycling pathway is not necessary for AcMNPV infection. In contrast, disruption of Rab11 function or expression (with DN Rab11 or Rab11-targeted RNAi) inhibited AcMNPV internalization and infectious virus production (Figs. 5 and 6). Rab11 is a prominent marker of RE. In many cell types, REs are clustered in the perinuclear-localized endocytic recycling compartment (ERC), which serves as the center station for regulation of endocytic recycling. Rab11 regulates EE relocating or EE-derived vesicles trafficking to ERC, where they deliver the cargo to RE. Then RE-derived vesicles pinch off and transport the recycling cargo to the plasma membrane (Naslavsky and Caplan, 2018). The inhibitory effect of disruption of Rab11 on AcMNPV entry may be interpreted by a slowing of cargoes trafficking from EE to ERC or RE, thereby reducing the amount of virions internalized through the recycling endosomal pathway.

Several recent studies found that Rab5 and Rab11 play regulatory roles in assembly and/or budding and release of enveloped DNA and RNA viruses in different viral families (Bruce et al., 2012; Vale-Costa and Amorim, 2016). Therefore we asked whether the negative effects of DN Rab5 and Rab11 on infectious AcMNPV production may also result from less efficient BVs release. To experimentally circumvent the effects of DN Rab5 and Rab11 on BVs entry by endocytosis, we initiated infections by either low-pH triggered direct fusion of BVs at the plasma membrane, or by transfecting cells with viral bacmid DNAs. In those experiments, DN Rab5 and DN Rab11 had no notable effect on production of infectious progeny BVs (Fig. 7A and B, panel c), suggesting that Rab5-and Rab11-dependent pathways are not required for AcMNPV egress.

In summary, our results indicate that cellular Rab5 and Rab11 are important for AcMNPV BVs entry by clathrin-mediated endocytosis in Sf9 cells. It is of note that the results of our detailed analysis in permissive Sf9 cells, is consistent with the identification of Rab5 and Rab11 in a recent RNAi screen of secretory pathway proteins involved in AcMNPV BVs entry in a Drosophila melanogaster cell line DL1, which is non-permissive for AcMNPV replication (Hodgson et al., 2019). In contrast, a remarkable difference observed is that RNAi knockdown or overexpression of the DN construct of Rab7 had no effect on AcMNPV entry into Sf9 cells in the current study, whereas Rab7 knockdown resulted in a dramatic reduction of the virus entry in Drosophila cells in the prior study (Hodgson et al., 2019). In addition to this difference, the dependence of different ESCRT components was also observed in assessing AcMNPV entry into Drosophila cells and lepidopteran Sf9 cells in prior studies (Hodgson et al., 2019; Yue et al., 2018). RNAi knockdown of the ESCRT-I component Vps28 or the ESCRT-III component Vps2B, Vps20, Vps24, or Vps46 did not affect AcMNPV entry into Drosophila cells (Hodgson et al., 2019), whereas the disruption of those ESCRT-I and ESCRT-III components by RNAi or overexpression DN protein dramatically inhibited the virus entry into Sf9 cells (Yue et al., 2018). Together, these studies suggest that the requirements of cellular factors and the potential complex interaction of those factors for efficient entry of AcMNPV into non-permissive cells (dipteran DL1) and permissive cells (lepidopteran Sf9) are substantially different. Because of the complexity of cellular vesicle transport, and the multiple and interlaced functions of many of the important components of these systems (such as the Rab proteins, ESCRT and SNARE complexes), understanding how baculoviruses navigate vesicular transport during entry into permissive and non-permissive insect cells will be an ongoing challenge but one of immense importance in understanding successful viral infections.

Funding

This work was supported by grants from the National Natural Science Foundation of China (No. 31672082, 31272088) to ZL and

grants from the United States Department of Agriculture (2015-67013-23281) and National Science Foundation (1653021) to GB.

Declaration of competing interest

Authors declare no conflict of interest.

Acknowledgement

The authors thank Taro Ohkawa and Matthew Welch for the kind gift of virus AcMNPV-3mC.

Appendix A. Supplementary data

Supplementary data to this article can be found online at https://doi.org/10.1016/j.ibmb.2020.103409.

References

- Antonny, B., Burd, C., De Camilli, P., Chen, E., Daumke, O., Faelber, K., Ford, M., Frolov, V.A., Frost, A., Hinshaw, J.E., Kirchhausen, T., Kozlov, M.M., Lenz, M., Low, H.H., McMahon, H., Merrifield, C., Pollard, T.D., Robinson, P.J., Roux, A., Schmid, S., 2016. Membrane fission by dynamin: what we know and what we need to know. EMBO J. 35. 2270–2284.
- Blissard, G.W., Theilmann, D.A., 2018. Baculovirus entry and egress from insect cells. Annu. Rev. Virol. 5, 113–139.
- Blissard, G.W., Wenz, J.R., 1992. Baculovirus gp64 envelope glycoprotein is sufficient to mediate pH-dependent membrane fusion. J. Virol. 66, 6829–6835.
- Bruce, E.A., Stuart, A., McCaffrey, M.W., Digard, P., 2012. Role of the Rab11 pathway in negative-strand virus assembly. Biochem. Soc. Trans. 40, 1409–1415.
- Buczynski, G., Bush, J., Zhang, L., Rodriguez-Paris, J., Cardelli, J., 1997. Evidence for a recycling role for Rab7 in regulating a late step in endocytosis and in retention of lysosomal enzymes in Dictyostelium discoideum. Mol. Biol. Cell 8, 1343–1360.
- Chambers, A.C., Aksular, M., Graves, L.P., Irons, S.L., Possee, R.D., King, L.A., 2018.

 Overview of the baculovirus expression system. Curr. Protein Pept. Sci. 91, 541–546.
- Chen, Y.R., Zhong, S., Fei, Z., Gao, S., Zhang, S., Li, Z., Wang, P., Blissard, G.W., 2014. Transcriptome responses of the host Trichoplusia ni to infection by the baculovirus Autographa californica multiple nucleopolyhedrovirus. J. Virol. 88, 13781–13797.
- Cormont, M., Bortoluzzi, M.N., Gautier, N., Mari, M., van Obberghen, E., Le Marchand-Brustel, Y., 1996. Potential role of Rab4 in the regulation of subcellular localization of Glut4 in adipocytes. Mol. Cell Biol. 16, 6879–6886.
- Dong, S., Wang, M., Qiu, Z., Deng, F., Vlak, J.M., Hu, Z., Wang, H., 2010. Autographa californica multicapsid nucleopolyhedrovirus efficiently infects Sf9 cells and transduces mammalian cells via direct fusion with the plasma membrane at low pH. J. Virol. 84, 5351–5359.
- Fan, Q., Kopp, S.J., Connolly, S.A., Longnecker, R., 2017. Structure-based mutations in the herpes simplex virus 1 glycoprotein B ectodomain arm impart a slow-entry phenotype. mBio 8. https://doi.org/10.1128/mBio.00614-17.
- Goley, E.D., Ohkawa, T., Mancuso, J., Woodruff, J.B., D'Alessio, J.A., Cande, W.Z., Volkman, L.E., Welch, M.D., 2006. Dynamic nuclear actin assembly by Arp2/3 complex and a baculovirus WASP-like protein. Science 314, 464–467.
- Goody, R.S., Muller, M.P., Wu, Y.W., 2017. Mechanisms of action of Rab proteins, key regulators of intracellular vesicular transport. Biol. Chem. 398, 565–575.
- Guo, Y., Yue, Q., Gao, J., Wang, Z., Chen, Y.R., Blissard, G.W., Liu, T.X., Li, Z., 2017. Roles of cellular NSF protein in entry and nuclear egress of budded virions of Autographa californica multiple nucleopolyhedrovirus. J. Virol. 91. https://doi.org/10.1128/JVI. 01111-17.
- Harrison, R.L., Herniou, E.A., Jehle, J.A., Theilmann, D.A., Burand, J.P., Becnel, J.J., Krell, P.J., van Oers, M.M., Mowery, J.D., Bauchan, G.R., Ictv Report, C., 2018. ICTV virus taxonomy profile: Baculoviridae. J. Gen. Virol. 99, 1185–1186.
- Hefferon, K.L., Oomens, A.G., Monsma, S.A., Finnerty, C.M., Blissard, G.W., 1999. Host cell receptor binding by baculovirus GP64 and kinetics of virion entry. Virology 258, 455–468.
- Hodgson, J.J., Buchon, N., Blissard, G.W., 2019. Identification of insect genes involved in baculovirus AcMNPV entry into insect cells. Virology 527, 1–11.
- Huotari, J., Helenius, A., 2011. Endosome maturation. EMBO J. 30, 3481–3500.
- Kadlec, J., Loureiro, S., Abrescia, N.G., Stuart, D.I., Jones, I.M., 2008. The postfusion structure of baculovirus gp64 supports a unified view of viral fusion machines. Nat. Struct. Mol. Biol. 15, 1024–1030.
- Kaksonen, M., Roux, A., 2018. Mechanisms of clathrin-mediated endocytosis. Nat. Rev. Mol. Cell Biol. 19, 313–326.
- Klopper, T.H., Kienle, N., Fasshauer, D., Munro, S., 2012. Untangling the evolution of Rab G proteins: implications of a comprehensive genomic analysis. BMC Biol. 10, 71.
- Kummel, D., Ungermann, C., 2014. Principles of membrane tethering and fusion in endosome and lysosome biogenesis. Curr. Opin. Cell Biol. 29, 61–66.
- Lee, R.C., Hapuarachchi, H.C., Chen, K.C., Hussain, K.M., Chen, H., Low, S.L., Ng, L.C., Lin, R., Ng, M.M., Chu, J.J., 2013. Mosquito cellular factors and functions in mediating the infectious entry of chikungunya virus. PLoS Neglected Trop. Dis. 7, e2050.
- Li, Z., Blissard, G.W., 2012. Cellular VPS4 is required for efficient entry and egress of budded virions of Autographa californica multiple nucleopolyhedrovirus. J. Virol. 86,

- 459-472
- Li, Z., Zhao, K., Lan, Y., Lv, X., Hu, S., Guan, J., Lu, H., Zhang, J., Shi, J., Yang, Y., Song, D., Gao, F., He, W., 2017. Porcine hemagglutinating encephalomyelitis virus enters Neuro-2a cells via clathrin-mediated endocytosis in a Rab5-, cholesterol-, and pH-dependent manner. J. Virol. 91. https://doi.org/10.1128/JVI.01083-17.
- Long, G., Pan, X., Kormelink, R., Vlak, J.M., 2006. Functional entry of baculovirus into insect and mammalian cells is dependent on clathrin-mediated endocytosis. J. Virol. 80, 8830–8833.
- Luckow, V.A., Lee, S.C., Barry, G.F., Olins, P.O., 1993. Efficient generation of infectious recombinant baculoviruses by site-specific transposon-mediated insertion of foreign genes into a baculovirus genome propagated in Escherichia coli. J. Virol. 67, 4556. 4570.
- Macia, E., Ehrlich, M., Massol, R., Boucrot, E., Brunner, C., Kirchhausen, T., 2006. Dynasore, a cell-permeable inhibitor of dynamin. Dev. Cell 10, 839–850.
- Mercer, J., Schelhaas, M., Helenius, A., 2010. Virus entry by endocytosis. Annu. Rev. Biochem. 79, 803–833.
- Mueller, J., Pfanzelter, J., Winkler, C., Narita, A., Le Clainche, C., Nemethova, M., Carlier, M.F., Maeda, Y., Welch, M.D., Ohkawa, T., Schmeiser, C., Resch, G.P., Small, J.V., 2014. Electron tomography and simulation of baculovirus actin comet tails support a tethered filament model of pathogen propulsion. PLoS Biol. 12, e1001765.
- Naslavsky, N., Caplan, S., 2018. The enigmatic endosome-sorting the ins and outs of endocytic trafficking. J. Cell Sci. 131, jcs216499. https://doi.org/10.1242/jcs. 216409
- Ohkawa, T., Volkman, L.E., Welch, M.D., 2010. Actin-based motility drives baculovirus transit to the nucleus and cell surface. J. Cell Biol. 190, 187–195.
- Qin, F., Xu, C., Hu, J., Lei, C., Zheng, Z., Peng, K., Wang, H., Sun, X., 2019. Dissecting the cell entry pathway of baculovirus by single-particle tracking and quantitative electron microscopic analysis. J. Virol. 93. https://doi.org/10.1128/JVI.00033-19.

- Rohrmann, G., 2019. Baculovirus Molecular Biology, fourth ed. National Center for Biotechnology Information (US), Bethesda (MD) [Internet].
- Schindelin, J., Arganda-Carreras, I., Frise, E., Kaynig, V., Longair, M., Pietzsch, T., Preibisch, S., Rueden, C., Saalfeld, S., Schmid, B., Tinevez, J.Y., White, D.J., Hartenstein, V., Eliceiri, K., Tomancak, P., Cardona, A., 2012. Fiji: an open-source platform for biological-image analysis. Nat. Methods 9, 676–682.
- Stenmark, H., Parton, R.G., Steele-Mortimer, O., Lutcke, A., Gruenberg, J., Zerial, M., 1994. Inhibition of rab5 GTPase activity stimulates membrane fusion in endocytosis. EMBO J. 13, 1287–1296.
- Ullrich, O., Reinsch, S., Urbe, S., Zerial, M., Parton, R.G., 1996. Rab11 regulates recycling through the pericentriolar recycling endosome. J. Cell Biol. 135, 913–924.
- Vale-Costa, S., Amorim, M.J., 2016. Recycling endosomes and viral infection. Viruses 8, 64.
- Volkman, L.E., Goldsmith, P.A., 1985. Mechanism of neutralization of budded Autographa californica nuclear polyhedrosis virus by a monoclonal antibody: inhibition of entry by adsorptive endocytosis. Virology 143, 185–195.
- Wollert, T., Hurley, J.H., 2010. Molecular mechanism of multivesicular body biogenesis by ESCRT complexes. Nature 464, 864–869.
- Yue, Q., Yu, Q., Yang, Q., Xu, Y., Guo, Y., Blissard, G.W., Li, Z., 2018. Distinct roles of cellular ESCRT-I and ESCRT-III proteins in efficient entry and egress of budded virions of Autographa californica multiple nucleopolyhedrovirus. J. Virol. 92. https:// doi.org/10.1128/JVI.01636-17.
- Zhao, M., Brunger, A.T., 2016. Recent advances in deciphering the structure and molecular mechanism of the AAA+ ATPase N-ethylmaleimide-sensitive factor (NSF). J. Mol. Biol. 428, 1912–1926.
- Zhou, J., Blissard, G.W., 2008. Identification of a GP64 subdomain involved in receptor binding by budded virions of the baculovirus Autographica californica multicapsid nucleopolyhedrovirus. J. Virol. 82, 4449–4460.